2024, 9(4s)

e-ISSN: 2468-4376

https://www.jisem-journal.com/

Research Article

Enhanced Zeta Converter Topology for High Voltage Conversion in PV Connected Grid Systems

Deepti Prasanna Tata^{1,*}, R. Sripriya², N. Bhupesh Kumar³
¹Research Scholar, Department of Electrical and Electronics Engineering, Annamalai University,
Annamalai Nagar, Chidambaram, Tamil Nadu - 608002

² Assistant Professor, Department of Electrical Engineering, Annamalai University, Annamalai Nagar, Chidambaram, Tamil Nadu – 608002

³ Professor, Department of Electrical and Electronics Engineering, Malla Reddy (MR) Deemed to be University, Hyderabad, Telangana, India

* Assistant Professor, Department of Electrical and Electronics Engineering, Sir C R Reddy College of Engineering, Eluru, Andhra Pradesh 534007 *Corresponding Email: tata.deepti@gmail.com

ARTICLE INFO

ABSTRACT

Received: 12 Oct 2024

Revised: 27 Nov 2024

Accepted: 24 Dec 2024

A DC-DC converter known as a "zeta converter" can be used in various power electronics applications to offer a voltage step-up (boost) or step-down (buck) function. The circuit became more complicated due to the numerous switched capacitor cells needed for the vast step-up conversion. Therefore, the research presents an advanced high step-up Zeta converter explicitly designed for photovoltaic (PV) applications, particularly in grid-connected systems where solar energy production can fluctuate. This improved converter maximises system efficiency and energy production by effectively controlling a broad input voltage range while optimising energy extraction from the PV array. It has near-unity power factor correction, which enhances power quality and makes grid integration easier by adjusting the input current to match the input voltage. The design minimises voltage spikes, switching noise, and electromagnetic interference (EMI) by utilising zero-voltage switching (ZVS) and interleaved operation. This improves system reliability and complies with regulatory standards for electromagnetic compatibility. Furthermore, a proportionalintegral-differential (PID) controller maximises voltage output by lowering component stress and increasing overall efficiency. As a result, the implementation includes significant results such that the output voltage of 513V, output current of 9.15A, power of 4693W and a power factor of 98.7, THD waveform based on voltage, current are 0.0009 volts, 0.01157 amperes. Due to its efficiency, adaptability, and simplicity, the converter is a valuable tool for many applications beyond grid-connected photovoltaic systems. This helps to promote sustainable energy development and the integration of renewable energy sources.

Keywords: Enhanced high step-up Zeta converter, Electric vehicles, Grid-connected PV systems, Power factor, Electromagnetic interference emissions.

1. INTRODUCTION

For many applications, to attain an output voltage of 300-400 V, renewable energy sources, including solar & fuel cells, require sizeable step-up dc/dc switch-mode converters [1]. Alternative energy sources must be created to keep up with the rising power demand. Renewable energy sources have emerged as the best option to offer clean energy sustainably without causing environmental pollution. Furthermore, the fact that there used to be a crude oil-based power plant made it rare because excessive use of the resource harmed the environment. Politicians and scientists were

2024, 9(4s)

e-ISSN: 2468-4376

https://www.jisem-journal.com/

Research Article

inspired by this fact to investigate renewable energy sources for power plants [22]. To attain an output voltage of 300-400 V, renewable energy sources, including solar & fuel cells, require sizeable step-up dc/dc switch-mode converters [2]. These renewable energy sources' inherent voltage levels were substantially lesser and unreliable. As a result, to convert greater voltage into grid supply, a high boost-up converter must retain & enhance the low-voltage renewable input energy from the source [3].

These various advancements, in addition to DC/DC converters, provide higher voltage conversion ratios. In this case, one option is to employ the switched-capacitor converters analysed. The authors developed a few design concepts that were useful in generating various switched-capacitor converters, but they still needed to be improved in some critical regions [4]. The term "isolated type" in a DC-DC converter describes an electrical barrier between the device's input and output sides. High-frequency transformers are used to create this barrier. It functions as a high-voltage conversion device and can be configured positively or negatively like a flyback converter [23]. Other required performance characteristics of these converters include stresses caused by low voltage and current, high conversion ratio, common ground, excellent efficiency & cheap rate [5]. In addition, the need for non-isolated converters with straightforward structures, improved efficiency, and reduced implementation costs is continuously rising [6].

A step-up voltage gain from renewable sources can produced by the traditional boost converter, which has a straightforward design and constant input current. However, switching and diode reverse recovery losses prevent it from making an excellent high-voltage gain [7, 8]. Conventional converters must be improved to obtain a significant voltage gain, exceptional efficiency, and a tolerable duty ratio [9]. Contrarily, the switched capacitor approach results in substantial current transients and significant conduction losses in the switch [10]. In addition, the massive step-up conversion required many switched capacitor cells, making the circuit more complex [11]. Therefore, creating a novel converter with high efficiency is essential in light of PV-connected grid systems. They stemsosed system's contribution is,

- The proposed converter achieves a power factor close to unity by matching input current with voltage, reducing harmonic content, lowering reactive power, and improving system efficiency.
- This architecture effectively handles various input voltages, ensuring optimal performance under varying environmental conditions, making PV systems more reliable and adaptable to changes in sunlight intensity.
- In grid-connected contexts, interleaved operation in converters reduces electromagnetic interference (EMI) emissions by minimising switching noise and voltage spikes. This is important for preserving the integrity of control systems and communication.
- The converter's effectiveness extends beyond photovoltaic systems, as it can supply an output voltage more significant than the input voltage.
- The suggested architecture reduces electromagnetic interference, maximises energy transfer, and minimises losses in PV systems to increase power conversion efficiency. This makes it appropriate for both residential and commercial applications.

The format of this document is as listed below: The literature reviews for various research projects are summarized in the second part. The overall plan is described in Segment 3. Segment 4 presents the findings and comments. The conclusion is disclosed in Segment 5. The sources for this study are listed in Section 6.

2. LITERATURE REVIEW

This study provides features of Zeng et al. [12] with an isolated four-port bidirectional DC-DC converter for integrating an integrated power system. The converter's key strengths are its two bidirectional ports, which have the fewest switches and allow system-level power flow management, such as transmitting (or absorbing) power to (or from) the DC link. The experiment's findings

2024, 9(4s)

e-ISSN: 2468-4376

https://www.jisem-journal.com/

Research Article

supported studies into the operating theory, Zero Voltage Switching (ZVS) settings, power curves, and operational scenarios. The converter can operate & switch between grid-connected and freestanding modes in line with the accessibility of the micro-grid with properly constructed and configured controllers.

Xiaodong et al. [13], The Dual-Active-Bridge Isolated Bidirectional DC-DC Converter (DAB-IBDC) is recommended for use in DC distribution networks to provide galvanic isolation, voltage conversion, power transfer, & bus connection. This study investigates the effects of phase-shift control on DAB-IBDC efficacy, current stress, & power transmission characteristics. Then, using dual-phase-shift (DPS), a multi-objective optimum control approach is designed to optimize all three aspects simultaneously. DPS control achieves lower HFL reactive power, lower current stress, & greater DAB-IBDC efficiency than single-phaseshift (SPS) control and maximizes all three properties simultaneously.

Salim et al. [14] proposed three DC-DC converters: Flyback-based converter, interleaved boost converter, & traditional Boost converter. Higher power and lower voltages were anticipated for renewable energy power systems. The converters, as well as the PSpice configuration, have been built. Furthermore, the only improved circuit to employ is to expand manufacturing quality and, by extension, the effectiveness of renewable energy systems. The simulation results demonstrate that the Flyback-based converter is the most excellent way to link lower-voltage stacked fuel cell & PV array modules to the 220.00 V AC grid. In brief, the Flyback-based converter is the best architecture because of its higher switching frequency, efficiency, and reduced device stress. Additionally, the best way to boost converter efficiency is with GaN-based technology.

Azmoon et al. [15] presented a non-isolated multiple input multiple output (MIMO) DC-DC converter in this research with numerous input and output ports and a sizeable step-up capacity, as recommended. The proposed converter requires only two switches suitable for renewable energy applications. Because a recommended converter only allows two working modes for each duty cycle, its control technique is simple. The suggested design has several advantages, including the capacity to provide significant voltage increases with a limited amount of duty cycle, the ease with which each duty cycle may be modified, and the low per-unit peak voltage stress (PPVS) inflicted on semiconductors. Continuous conduction mode is used for the operating principles, steady-state analysis, & extraction of voltage and current equations.

Jiahong Ning et al. [16] recommended a new 4-port bidirectional DC-DC converter for controlling power utilizing renewable energy, microgrids, batteries, and sources. The suggested converter has been used to interface a hybrid system with various energy sources, such as a battery, a WTG, and a PV panel. Simulation and experimentation have been conducted to verify the converter's operating principle. The outcomes demonstrated that the measured fundamental waveforms accurately mirrored the analysis. The proposed converter can switch operating modes by adjusting the phase-shift angle between the low-voltage side (LVS) switches and high-voltage sides (HVS). Participation in system-level control is made feasible by the bidirectional power flow.

Chandran et al. [17] suggested the three-port non-isolated zeta converter. The battery and PV sources are the two primary embodiments of the suggested three-port zeta converter. The control strategy that has been outlined highlights how adaptable the task is under various limitations. The converter may provide a significant output voltage even with a low input voltage. It has been determined what the efficiency, voltage gain, current and voltage ripples, and switch voltage stress are. The suggested converter is a good fit for LED lighting applications and biomedical devices that demand input voltages with low ripple. It has a high voltage gain and a low output voltage ripple.

3. ENHANCED HIGH STEP-UP ZETA CONVERTER ARCHITECTURE

The proposed research introduces an enhanced high step-up Zeta converter topology specifically tailored for PV applications, addressing critical challenges while leveraging the advantages

2024, 9(4s)

e-ISSN: 2468-4376

https://www.jisem-journal.com/

Research Article

of the Zeta converter. In the context of grid-connected PV systems, as shown in Figure 1, where energy production can vary due to changing solar conditions, the ability of the converter to handle a wide input voltage range is crucial. This feature ensures optimal energy extraction from the PV array, maximizing the system's efficiency and yield. Additionally, the converter actively shapes the input current to be in phase with the input voltage, achieving near-unity power factor correction. By minimizing harmonic content and improving power quality, the converter facilitates smooth integration with the grid, reducing energy losses and ensuring stable operation.

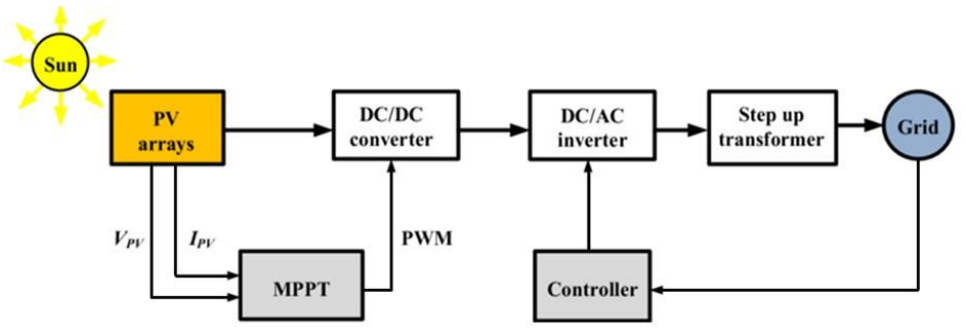


Figure 1: Grid connected PV system with proposed converter and controller

Furthermore, the interleaved operation and zero-voltage switching (ZVS) employed in the converter design minimizes switching noise, voltage spikes, and electromagnetic interference (EMI) emissions. This enhances system reliability and ensures compliance with stringent regulatory standards governing electromagnetic compatibility. A PID controller for voltage control further enhances the converter's performance by optimizing voltage output, reducing stress on critical components, and improving overall efficiency. The proposed converter's simplicity, efficiency, and adaptability make it suitable for various applications beyond grid-connected PV systems, contributing to advancing renewable energy integration and developing sustainable energy systems.

3.1. Design of PV Module

Photovoltaic power generation is the main power supply for the DC micro grid, which is controlled to achieve its MPP. Using the single-diode circuit to represent the PV array is common practice since it is simple and accurate. The single-diode structure is also called the five-parameter model. A photo-generated controller is shown in Figure 2 in parallel with a diode, series resistance, and parallel resistance representing power loss.

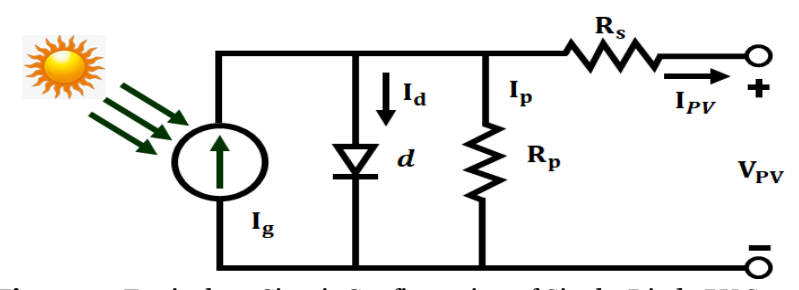


Figure 2: Equivalent Circuit Configuration of Single-Diode PV System

The inherent and non-linear expressions that determine solar cell's I-V characteristics are as follows in equation (1)(2)(3):

$$I_{PV} = I_g - I_d - \left(\frac{V_{PV} + R_s I_{PV}}{R_p}\right) \tag{1}$$

2024, 9(4s)

e-ISSN: 2468-4376

https://www.jisem-journal.com/

Research Article

$$I_d = I_0 \left[exp\left(\frac{q(V_{PV} + R_S I_{PV})}{nKT}\right) - 1 \right] \tag{2}$$

$$V_D = V_{PV} + R_s I_{PV} \tag{3}$$

Arrays consist of PV modules connected serially and parallel. The PV cells form a series string when arranged in series, and they form an array when connected in parallel. According to the following, these connections have an impact on the array's current-voltage relationship using equation (4) (5):

$$I_{PV} = N_{P}I_{g} - N_{P}I_{d} - \left(\frac{V_{PV} + \frac{N_{S}}{N_{P}}R_{S}I_{PV}}{\frac{N_{S}}{N_{P}}R_{p}}\right)$$
(4)

$$I_d = I_0 \left[exp\left(\frac{q\left(V_{PV} + \frac{N_S}{N_P}R_SI_{PV}\right)}{N_SnKT}\right) - 1 \right]$$
 (5)

From the expressions, the output voltage and current of the PV array are represented as V_{PV} and I_{PV} , charge of electron as q, cell connection in series and parallel as N_s and N_P , irradiance current as I_g , Boltzmann constant as K, temperature as T, shunt and series resistance as R_p and R_s , saturation current of diode as I_0 and ideality factor as n, respectively. PV systems produce variable amounts of power depending on solar temperature and irradiance. Therefore, Maximum Power Point Tracking (MPPT) maximises the power produced by PV cells. MPP is a variable operating point on the P-V curve that varies with irradiance and ambient temperature. As a result, a control scheme is used to drive the system to function at its best efficiency by controlling the PV array's duty cycle with an Integrated SEPIC-KY converter value. The following section details the operation and working conditions of the integrated SEPIC-KY converter.

3.2. High Step-Up Zeta Converter Architecture

Figure 3 shows connected boost and buck-boost converters in the cascade to produce high voltage gain. The step-up/down conversion ratio delivered by the converter when the main power MOSFET is under low voltage stress and the input current is constant is derived in equation (6):

$$G_{(ideal)} = \frac{D_{cycle}}{(1 - D_{cycle})^2} \tag{6}$$

In this instance, D_{cycle} represents the switch-duty cycle. This converter has a relatively low voltage conversion ratio despite having a quadratic voltage gain. Because of the RES's low voltage level, a step-up converter with an ultra-voltage gain is usually required. As was already noted, a straightforward and precise approach for increasing the converter's duty cycle without increasing the voltage conversion ratio is to use inductance efficiently to increase the gain and reduce the switching losses.

2024, 9(4s)

e-ISSN: 2468-4376

https://www.jisem-journal.com/

Research Article

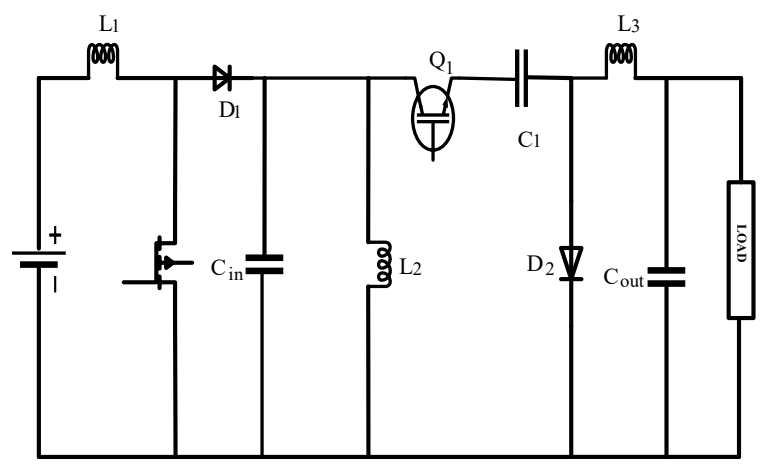


Figure 3: Topology of the proposed converter

The novel buck-boost converter was evaluated using the following criteria.

- All capacitors were intended to be of appropriate size, with almost constant voltages over a single switching cycle and negligible voltage ripples.
 - Semiconductor components, including diodes with switches, are all regarded as ideal.
- The proposed improved high step-up DC/DC converter includes an error-mitigating PID solution for each switching cycle.

A boost converter and a buck-boost converter are added to the standard Zeta converter to modify it. Combining the advantages of both converter types, this configuration seeks to achieve a significant voltage gain. By ensuring that the main power MOSFET functions under low voltage stress, the design contributes to increased dependability and reduced component stress. The converter's design maximises the use of inductors to boost voltage gain while limiting the increase in the duty cycle. By using inductance effectively, switching losses are reduced, and gain is increased. The converter's capacitors are all the right size to guarantee almost consistent voltages during a switching cycle with the fewest possible voltage waves. To simplify the analysis and concentrate on the fundamental performance of the converter, the design assumes that all semiconductor components, including switches and diodes, are perfect. An error-mitigating PID controller is included to control the converter's performance during each switching cycle.

3.2.1. Continuous Conduction Mode

The proposed topological operating concept in Continuous Conduction Mode (CCM) contains three-time intervals and fundamental waveforms for one period, together with each mode's current flow routes, shown in Figure 4. The following sentences analyse and completely describe the three modes in further detail:

2024, 9(4s)

e-ISSN: 2468-4376

https://www.jisem-journal.com/

Research Article

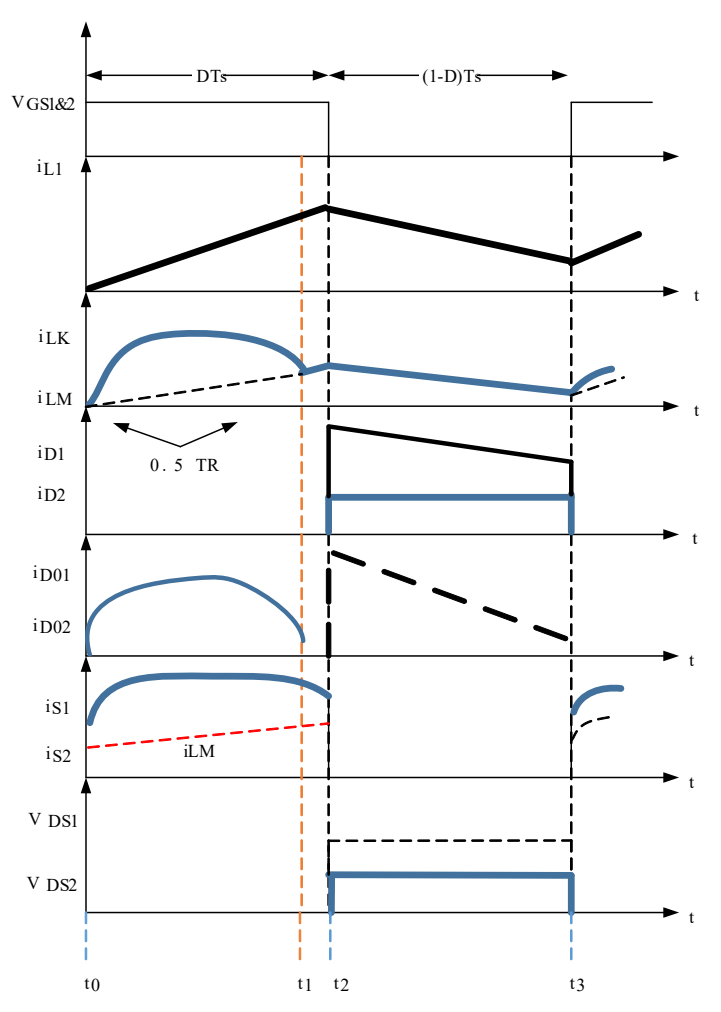


Figure 4: Waveforms of the introduced DC-DC

3.2.1.1. Mode 1

Power switches S1 is ON and S2 is OFF state in mode 1 which starts conducting simultaneously at time T = To, and diode D1 does not perform. In this mode, Figure 5 depicts the circuit's current flow path.

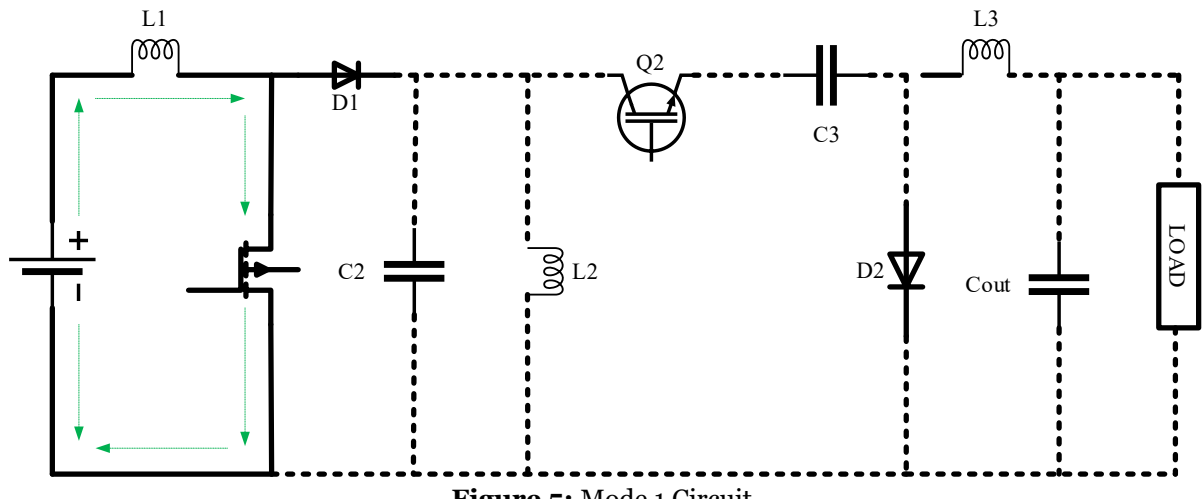


Figure 5: Mode 1 Circuit

2024, 9(4s)

e-ISSN: 2468-4376

https://www.jisem-journal.com/

Research Article

The input inductor L1 gets electricity from the input voltage source Vin when S1 is ON, and its current grows linearly. In this mode, the diode D1 blocks the current to pass through the following circuit by equation (7) (8) (9).

$$V_{L1} = V_{in} \tag{7}$$

$$iS_1 = iL_1 \tag{8}$$

$$iS_{1}' = iL_{1} + iL_{1}' \tag{9}$$

Thus, the currents run via the power switch S1, and with the help of the inductor L1, the current grows sinusoidal. It also minimizes the diode D1's reverse recovery loss and the power switches' turn-off state losses greatly. The current in the inductor increases linearly as a function of the voltages from the source.

3.2.1.2. Mode 2

Switch S_1 and S_2 is OFF, while D_1 conducts current. Figure 6 depicts the current flow's direction. L1 conducts the induced current via diode D1, while C_1 gets charged. Therefore, the following equation (10) (11) are appropriate:

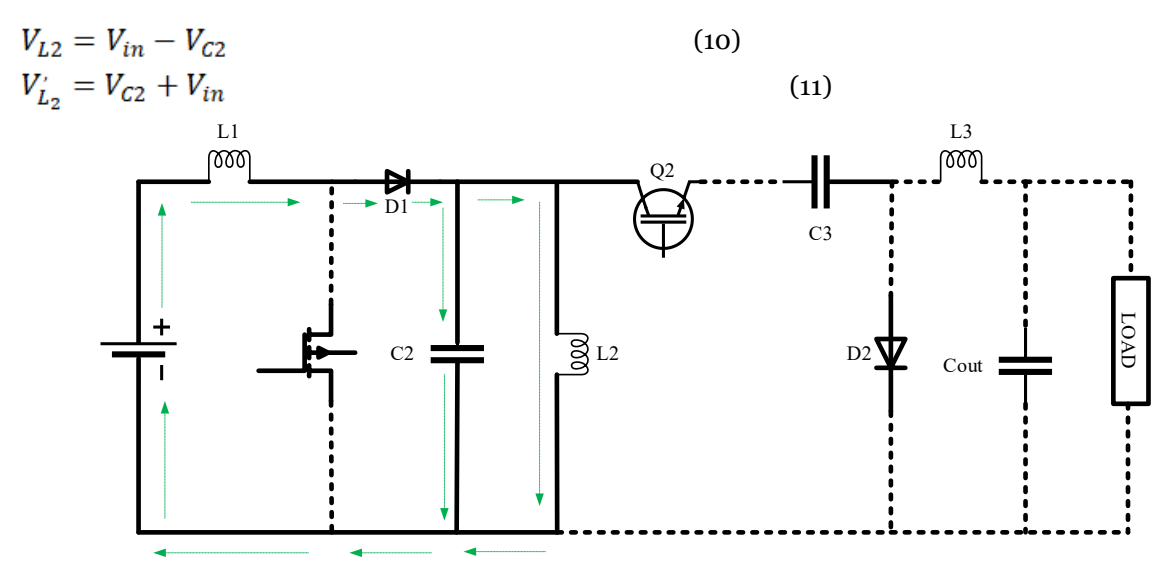


Figure 6: Mode 2 Circuit

3.2.1.3. Mode 3

Switch 1 is on and switch 2 is ON, while D1 conducts current and D2 is reverse biased. Demagnetization is applied to the inductors L2, L3, and L4. With the help of the inductor L2, the capacitor C2 gets charged. A discharge in capacitors C3 and C4 is shown in Figure 7.

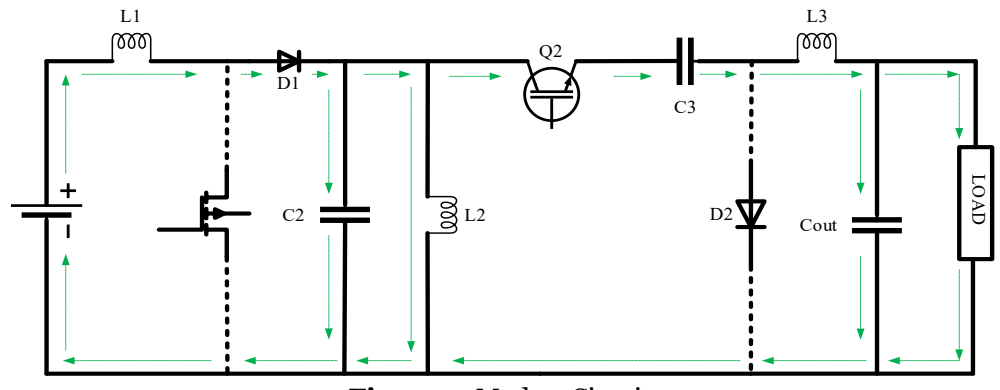


Figure 7: Mode 3 Circuit

2024, 9(4s)

e-ISSN: 2468-4376

https://www.jisem-journal.com/

Research Article

The following is how inductor voltages are derived in equation (12) (13) (14):

$$V_{L2} = V_{C3} - V_{C2} (12)$$

$$V_{L3} = -V_{C3} = -V_{C4} \tag{13}$$

$$V_{L4} = V_{C4} - V_0 \tag{14}$$

Finally, the following equation (15) provides the temporal formulation of a PID controller:

$$u(t) = K_p e(t) + K_i \int_0^{\tau} e(\tau) d\tau + K_d \frac{de(t)}{dt}$$
(15)

Where the error is represented by e(t), and u(t) stands for the control signal. The derivative gain is denoted by K (d). At the same time, Kp and Ki, respectively, are used in a form diagram for a parallel PID controller to show the benefits are proportionate and integral.

The discrete-time PID-controller form is given by equation (16):

$$u_k = K_p e_k + K_i \sum_{n=1}^k e_k + K_d (e_k - e_{k-1})$$
(16)

The following equation (17) known velocity form is used to create a discrete-time PID controller:

$$u_k = u_{k-1} + K_p(e_k - e_{k-1}) + K_i e_k + K_d(e_k - 2e_{k-1} + e_{k-2})$$
 (17)

Thus, the proposed converter is supposed to work optimally in the CCM and DCM states.

4. RESULTS AND DISCUSSION

The simulation results of the recommended converter with a connected grid system in the MATLAB environment are described in this section. It also looks at how well the outcomes perform compared to conventional converters.

4.1. Mathematical Analysis

4.1.1. Steady-state analysis:

Mode II in CCM operation has a brief time transition, which can be ignored. The voltage of the middle capacitors C_1 and C_2 is produced by applying the inductor volt-second balance concept to the input inductor (L_1) determined in equation (18),

$$V_{C1} = V_{C2} = \frac{V_{\text{in}}}{1 - D} \tag{18}$$

Where D represents the duty cycle of the power switches S1 and S2. The volt-second balance for L2 is used to explain the output half-stage voltage gains in CCM using equation (19)(20).

$$V_{C01} = \frac{(1+D)V_{\rm in}}{(1-D)^2} \tag{19}$$

$$V_{C02} = nk(V_{C1} + V_{C2}) = \frac{2nkV_{\rm in}}{(1-D)}$$
 (20)

2024, 9(4s)

e-ISSN: 2468-4376

https://www.jisem-journal.com/

Research Article

As a result of adding (19) and (20), the suggested converter's static voltage conversion ratio is as follows in equation (21):

$$M_{\text{CCM(ideal)}} = \frac{1+D+2nk(1-D)}{(1-D)^2}$$
 (21)

The proposed converter has much better coupling coefficients (k), frequent turns ratios of CI, and voltage gain ratios than the converter. If D=0.65 and n=1 are used in the suggested converter, the optimal voltage gain, for example, is M=18.77, three and a half times that of the converter (with M=5.3 in = 0.65). Furthermore, the leaky inductor's small coupling coefficients (k=0.9 and =0.8) can lower the voltage gain ratio. The conversion ratio is unaffected by this coefficient for low CI power rates. Hence, it can be set to one (k1) in this situation, eqn (22). The optimal voltage conversion ratio for the proposed converter is represented by the following equation (22):

$$M_{CCM}(ideal) = \frac{1 + D + 2n(1 - D)}{(1 - D)2}$$
 (22)

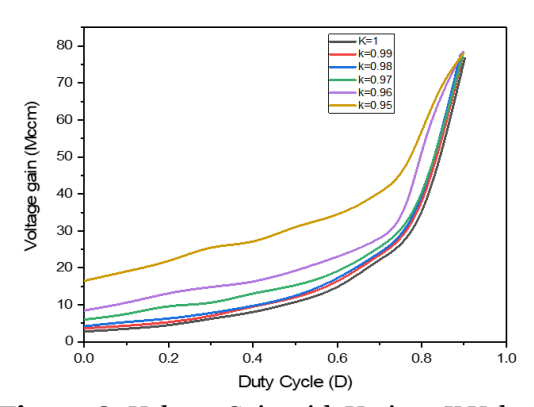


Figure 8: Voltage Gain with Various K Values

Additionally, the suggested converter's voltage conversion ratio develops exponentially with the duty cycle in semi-quadratic form and accordance with the turns-to-ratio of CI. The result is that this converter can convert voltage to extremely high levels, as shown in Figure 8.

In the case of L_1 and L_2 , the volt-sec balancing principle can be used; we obtain the equation (23)

$$\frac{1}{T_s} \left(\int_0^{DT_i} V_i dt + \int_{DT_t}^{T_4} (V_{C2} - V_{C1}) dt \right) = 0$$

$$\frac{1}{T_s} \left(\int_0^{DT_4} (V_i + V_{C1} - V_{C2} - V_{C3}) dt + \int_{DT_4}^{T_4} (-V_{C2}) dt \right) = 0$$
(23)

The voltage of C_1 , C_2 , & C_3 (V_{C1} , V_{C2} , & V_C) may be obtained as follows in equation (24):

$$V_{C2} = V_{C3} = \frac{DV_i}{1-D}$$
; $2V_{C1} = V_{C2}$ (24)

Using volt seconds balance, get the voltage transfer gain (M_{CCM}) using equation (25):

2024, 9(4s)

e-ISSN: 2468-4376

https://www.jisem-journal.com/

Research Article

$$\frac{1}{T_s} = \left(\int_0^{DT_t} (V_{Cl} + V_i - V_o) dt \int_{Dr_t}^{T_s} (V_{C3} - V_o) dt \right) = 0$$

$$M_{CCM} - \frac{V_o}{V_t} - \frac{2D}{1 - D} \tag{25}$$

The results demonstrate that the voltage improvement of the proposed converter is twice as significant as that of the Zeta converter. As a result, the voltage improvement of the converter is more critical than that of the Zeta converter, as shown in Figure 9.

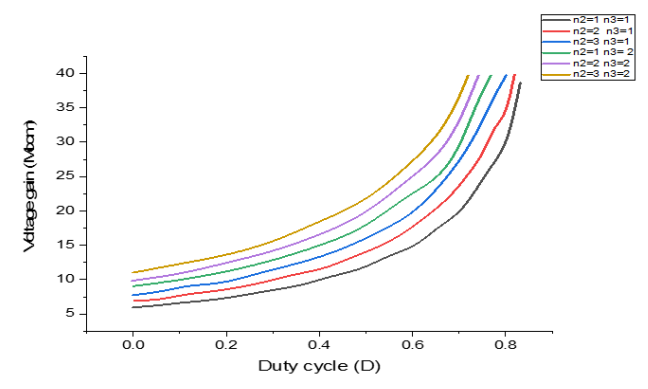


Figure 9: Voltage Gain curve

4.1.2. Current Calculation

Average currents of inductors I_{L2} , I_{L3} , and across capacitors C2 and C3 during switch ON period in mode 1 using equation (26) (27) (28).

$$I_{23} = \frac{(2D)V_1}{R(1-D)}$$

$$I_{CL,\infty n} = -\left(I_{L2} + \frac{(2D)V_1}{R(1-D)}\right)$$

$$I_{C2,an} = I_{C3,an} = I_{L,2}$$
(26)
$$(27)$$

Then, the mean current I_{Cl} , from capacitor C_1 in mode 2, the expressions are as follows in equation (29),

$$I_{C1,aff} = (I_{L,2} - I_{C2, off} - I_{C3, off} - I_{L,3})$$
(29)

Here, I_{C2} off is the mean current of C_2 and I_C off is the mean current of C_3 in mode 2 on the principle of ampere sec balance on C_1 , C_2 and C_3 . The expression framed is determined in equation (30).

$$\frac{1}{T_s} \left(\int_0^{DT_a} I_{C1,2,3,0n} dt + \int_{DT_a}^{T_a} I_{C1,2,3,ag'} dt \right) = 0$$
 (30)

By applying the expressions (27), (28), (29), (30) in expression (31), the mean current I_{C2} , on, I_{C3} , on of capacitors C_2 , C_3 , and the current $I_{1.2}$ of the inductor L_2 are organized as below in equation (31),

2024, 9(4s)

e-ISSN: 2468-4376

https://www.jisem-journal.com/

Research Article

$$I_{L2} = I_{C2,\infty 0} = I_{C3,\infty} = \frac{(2D)V_i}{R(1-D)}$$
 (31)

 I_{C1} is the mean current of the capacitor C_1 , as stated in equation (32).

$$I_{C1,\infty} - \frac{(-4D)V_i}{R(1-D)} \tag{32}$$

The inductor L1 means the current is expressed as equation (33),

$$I_{L,1} = I_{C1,\omega\pi} - \frac{(4D^2)V_i}{R(1-D)^2}$$
(33)

The current across the switch (S) & I_{D1} , I_{D2} (D₁, D₂) is the current stress across the diodes using equation (34) (35) (36).

$$I_{s} = I_{L,1} - I_{C1,a\omega} = \frac{(4D)V_{a}}{R(1-D)^{2}}$$
(34)

$$I_{D1} = I_{L2} - I_{C2,\alpha\theta} = \frac{V_t(2D)}{R(1-D)^2}$$
 (35)

$$I_{D2} = I_{L,2} - I_{C3,Ad} = \frac{V_l(2D)}{R(1-D)^2}$$
 (36)

The proposed converter will likely experience some conduction loss because its current stress is smaller than that of a traditional converter.

4.1.3. DCM Operation Condition

Mode I produces a half-stage voltage gain in DCM as equation (37)

$$M_{02} = \frac{v_{C02}}{v_{ln}} = 2n \left(\frac{1-D}{1+D}\right) M_{01} \tag{37}$$

The suggested converter's static voltage gain ratio in DCM is provided by equation (38)

$$M_{\text{DCM}} = M_{01} + M_{02} = M_{01} \left(1 + 2n \left(\frac{1-D}{1+D} \right) \right)$$
 (38)

The formula may be used to calculate DCM's half-stage voltage gain as a function of total voltage gain using equation (39).

$$M_{\rm D1} = \frac{M_{\rm DCM}}{1 + 2n\left(\frac{1-\rm D}{1+1}\right)} \tag{39}$$

The average input current (also known as input inductor current) is expressed as equation (40)

$$I_{\rm in} = \frac{V_{\rm in}DT_S}{2L_1}(D + \Delta_1) \tag{40}$$

The voltage gain of a DCM (M_{DCM}) converter is computed as a function of D, n, and Q by combining equations (35) and (40) to determine equation (41).

2024, 9(4s)

e-ISSN: 2468-4376

https://www.jisem-journal.com/

Research Article

$$Q = \frac{f_S L_1}{R} \tag{41}$$

In this graph, the voltage gain capabilities of DCM and CCM are contrasted concerning the duty cycle and various Q and n values. In DCM operation, the converter parameters impact the voltage gain ratio. (Q). Therefore, suggestions for DCM performance are scarce.

4.1.4. Efficiency and loss calculations:

Converter performance is significantly influenced by loss, which is an essential element. A converter's overall loss is determined by the quantity and kind of its component elements. So that the efficiency of the suggested converter may be specified, this section is dedicated to calculating switching and conduction losses. The equation represents RMS currents and power losses for L1 and L2 below by equation (42) (43) (44):

$$I_{L1} = \frac{DI_0}{(1-D)^2} \tag{42}$$

$$I_{L2} = \frac{I_0}{(1-D)} \tag{43}$$

$$P_{Ln} = \sum_{N=1}^{n} \left[r_{LN} I_{LN}^{2} + \left(K f^{a} B_{ac}^{\beta} W_{tfe} \right) (10^{-3}) \right]$$
 (44)

The output diode's power loss using equation [41] is provided by equation (45)

$$P_{Do} = V_F I_{Do, \text{ ave }} + r_D I_{Do}^2 + \frac{Q_{rr} V_D f}{4}$$
 (45)

Furthermore, the diode's RMS current is provided by equation (46)

$$I_{\rm Dn} = \sqrt{\frac{1}{T} \int_0^{(1-D)T} \left(\frac{I_i}{n}\right)^2} dt \tag{46}$$

Diode total power loss is represented as equation (47) (48)

$$P_{D(n)} = \sum_{N=1}^{n} \left[V_F I_{D(n),ave} + r_D I_{D(N)}^2 \right]$$

$$P_{Cw} = \sum_{n=1}^{n} r_{c=r_{ck}}^2$$
(48)

Furthermore, the RMS currents and power losses of Us1 and S2 were computed using equation (49) (50)

$$U_{s_1} = \sqrt{\frac{1}{T} \int_0^{or} (U_1 + i_{12})^2 dr}$$
 (49)

$$J_{s_2} = \sqrt{\frac{1}{T} \int_0^{\nu - 2\pi r} \left(\frac{2\pi - 1}{2\nu}, \right)^2 dt}$$
 (50)

The converter's overall power loss and efficiency are as follows by equation (51) (52):

2024, 9(4s)

e-ISSN: 2468-4376

https://www.jisem-journal.com/

Research Article

$$P_{\text{Lan}} = P_{L\omega} + P_{ln} + P_{con} + P_L + P_{\Delta n} + P_c$$
 (51)

$$q = \frac{P_{...}}{P_m + P_{C...n}} \times 100 \tag{52}$$

4.2. Simulation Output

According to the modelling results, steady-state oscillation is negligible at the maximum power point, which reduces energy loss and improves system effectiveness. The converter simulation results show three different step-up (boost) settings, as shown in Figure 8. In the present study, a constant temperature of 25 $^{\circ}$ C and a solar intensity value of about 1000 W/m2 is applied as input to the solar panel. The solar intensity is 800 W/m2 till 0.25 s, and then it increases to 1000 W/m2 at the time of 0.25 s.

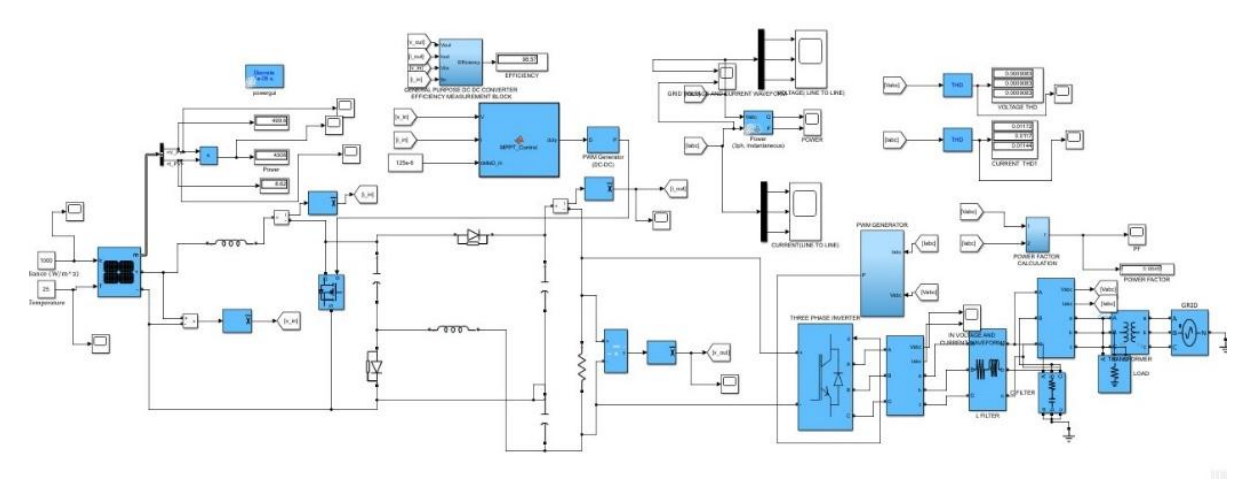


Figure 10: MATLAB Simulation of proposed model

The MATLAB Simulink model for the proposed converter is shown in Figure 10, which includes blocks representing the high step-up zeta converter architecture, power factor correction, interleaved operation, and PID controller. The high step-up zeta converter block simulated the voltage conversion process, considering the PV source and grid connection characteristics. The power factor correction block had adjusted the input current to align with the input voltage, aiming for a unity power factor. The interleaved operation was simulated by splitting the current into parallel paths, reducing switching noise and voltage spikes. It also improves thermal management by distributing the current across multiple phases. The PID controller block regulated the voltage output by continuously comparing the desired output voltage with the actual output and adjusting control signals accordingly. By integrating these components into a Simulink model, researchers simulated the behaviour of the proposed converter under various operating conditions, assessed its performance, and optimized its design parameters for improved efficiency and reliability in PV applications. The MATLAB Simulink model does not account for practical factors such as noise, operating frequency effects, and variations in load characteristics, which can significantly impact the real-world performance and efficiency of the proposed high step-up Zeta converter.

2024, 9(4s)

e-ISSN: 2468-4376

https://www.jisem-journal.com/

Research Article

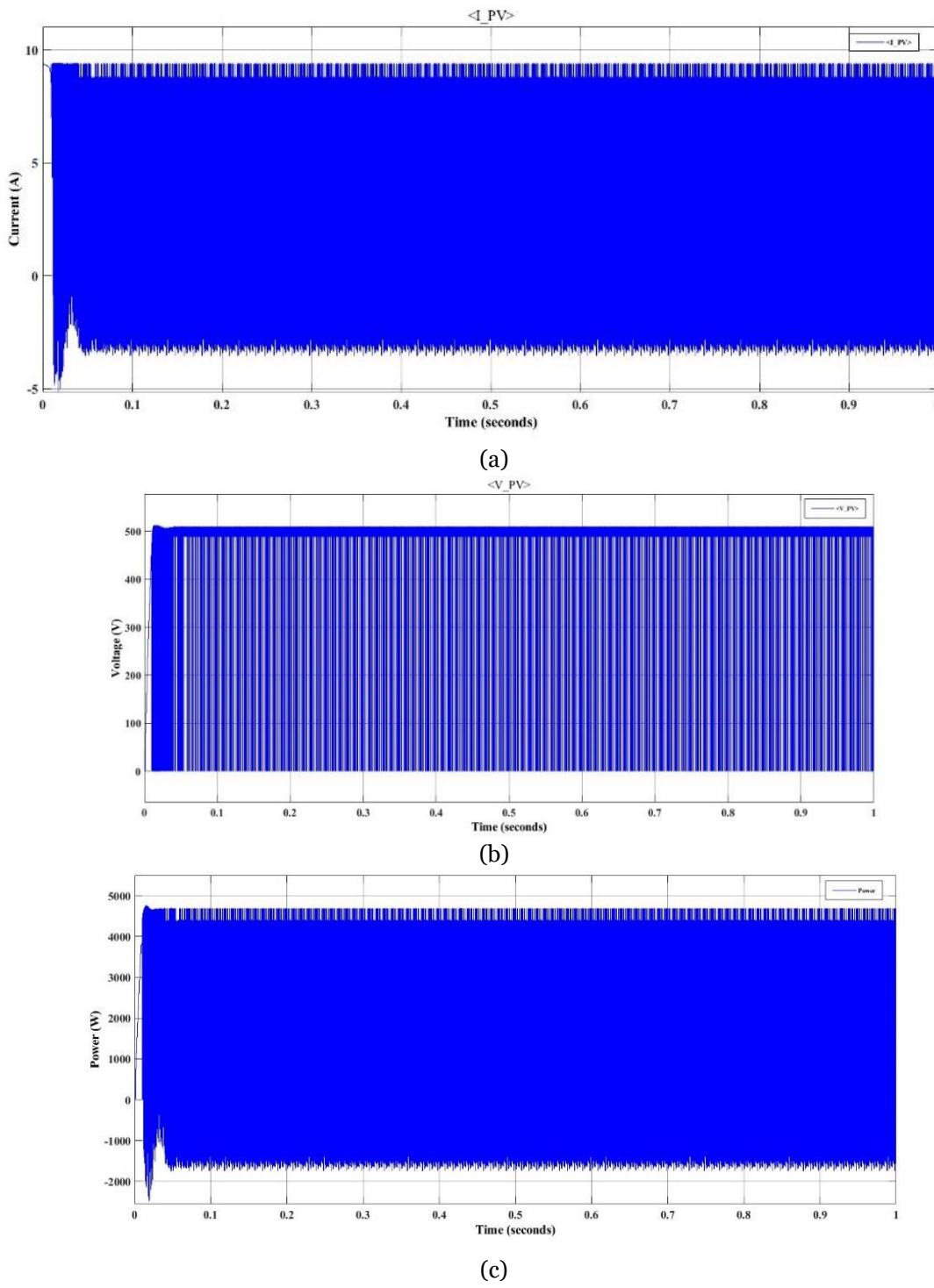


Figure 11: Input current, voltage and power from PV

Figure 11 shows the PV panel output current (2 a), voltage waveforms (2 b) and power waveform (2 c). Initially, the output voltage from the PV panel shows a voltage of 513 V and an output current of 9.15 A while maintaining a power of 4693 W. The performance of the PV panel may be significantly impacted by variables that are not considered, such as shifting temperature swings, shading, and changing environmental circumstances. Furthermore, the data only covers the initial

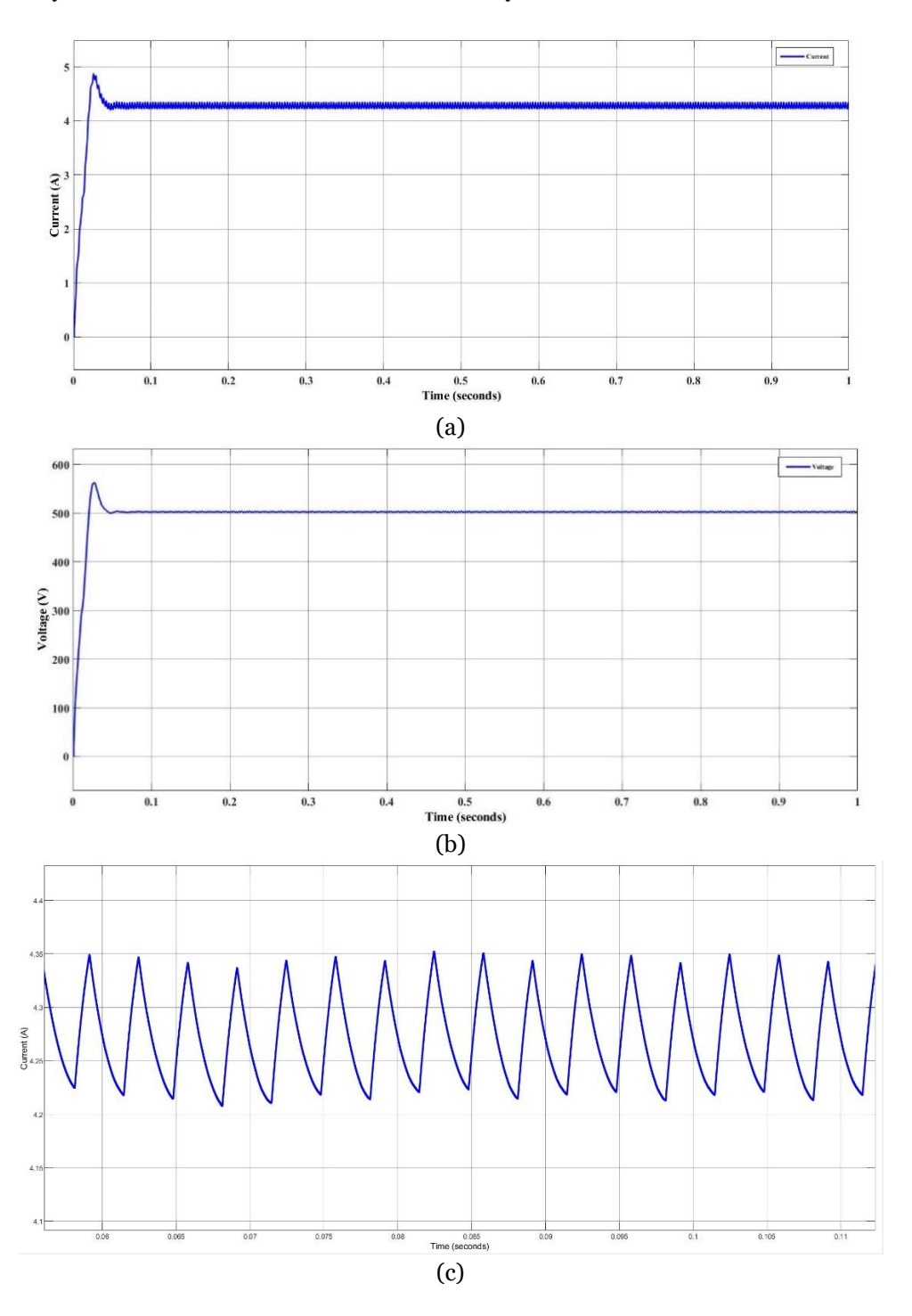
2024, 9(4s)

e-ISSN: 2468-4376

https://www.jisem-journal.com/

Research Article

conditions; it does not explain how the system performs over more extended periods or in the presence of dynamic variations in load and solar intensity.



2024, 9(4s) e-ISSN: 2468-4376

https://www.jisem-journal.com/

Research Article

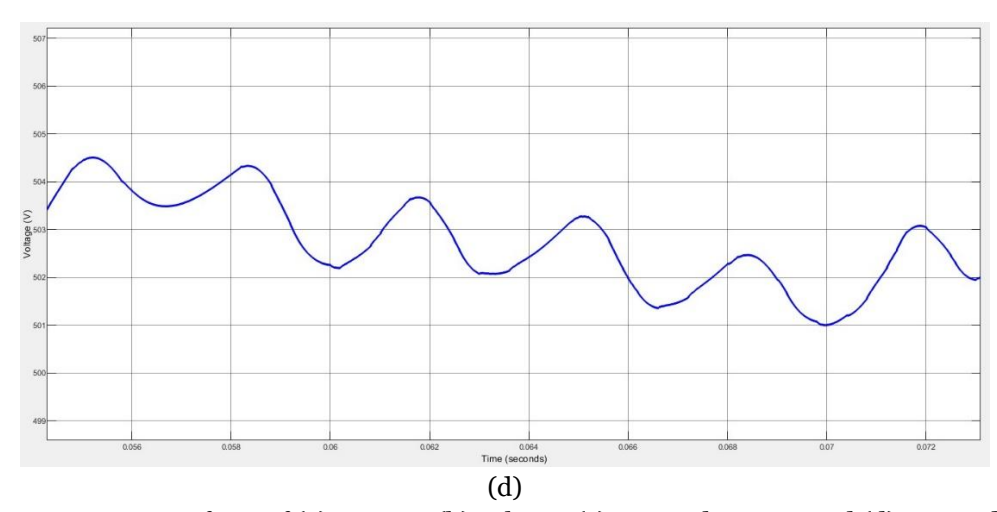


Figure 12 Output waveform of (a) current, (b) voltage, (c) Zoomed current and (d) Zoomed voltage from the proposed converter.

Figure 12 illustrates the voltage and current waveforms of the proposed enhanced high step-up Zeta converter for photovoltaic (PV) applications; several critical insights into its operation are revealed. The 500-volt voltage waveform demonstrates the converter's effective step-up capability, essential for powering loads that need greater voltages than the input source can deliver. Concurrently, the 4.53-ampere current waveform shows how well the converter aligns the input voltage and current to provide a power factor that is almost unity. This synchronisation guarantees strict power quality criteria are followed, reduces harmonic distortion, and increases system efficiency. The results are based on simulations, which may consider only some real-world factors that could affect the converter's performance, such as component tolerances, heat effects, and electromagnetic interference. Furthermore, the emphasis on reducing harmonic distortion and reaching near-unity power factors may need to be clarified for other essential performance indicators, like efficiency at partial load, long-term dependability, and the effect of ageing components.

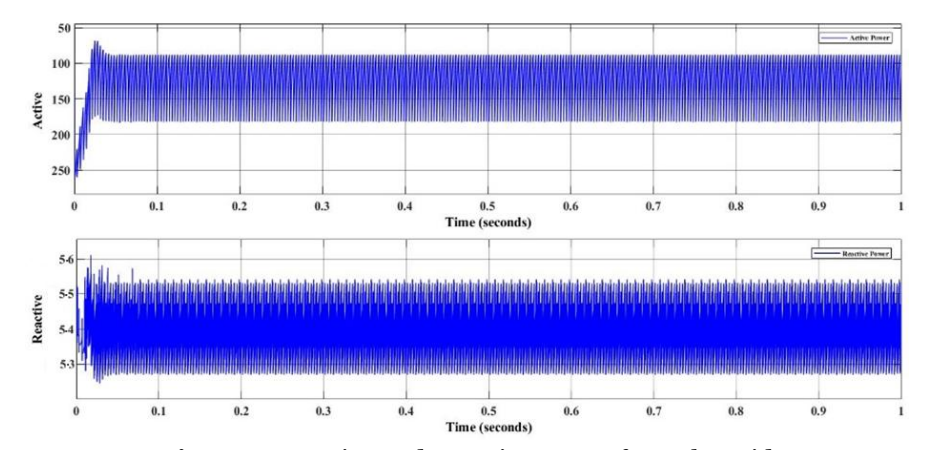


Figure 13: Active and Reactive power from the grid

Its active power range indicates a system's efficiency, which is 120 to 170 watts and reactive power with 5.3 to 5.5 volt-amperes reactive, as shown in Figure 13. Positive active power values indicate that the load primarily uses energy for practical work, typical for small to medium-sized electronic devices or appliances. Low reactive power values indicate minimal inductive or capacitive characteristics within the load, resulting in minimal energy cycling between the source and load. This results in a high power factor (close to unity), indicating efficient use of the supplied power.

2024, 9(4s)

e-ISSN: 2468-4376

https://www.jisem-journal.com/

Research Article

Furthermore, the analysis ignores other crucial elements that could affect the overall efficiency and dependability of the system, such as transient response, total harmonic distortion, and thermal management. Furthermore, real-world inefficiencies like losses in wiring, connectors, and other system components might be partially captured by simulation data.

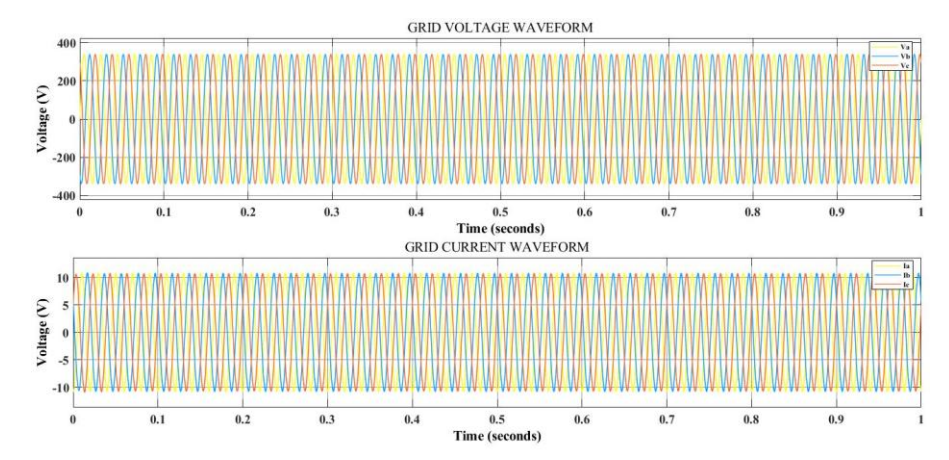


Figure 14: Voltage and Current waveform from grid

Figure 14 shows the grid voltage ranging from 350 to -350 volts and current fluctuating from 11 to -11 amperes in a waveform from a grid-connected system typically indicates a steady flow. In AC systems, both voltage and current waveforms are sinusoidal and oscillate between positive and negative peaks, reflected in the given ranges. This alternating nature is fundamental to operating AC power systems based on most residential and commercial grids. The amplitude of ± 350 volts suggests a high voltage level, line-to-line voltage in a three-phase system. A current amplitude of ± 11 amperes indicates the maximum flow of electric charge through the circuit, representing the current load capacity. The emphasis on current amplitude ignores possible variations brought on by changing system dynamics or loads over time. Moreover, the description ignores the effects of power factor variations, temperature, and ageing on system performance.

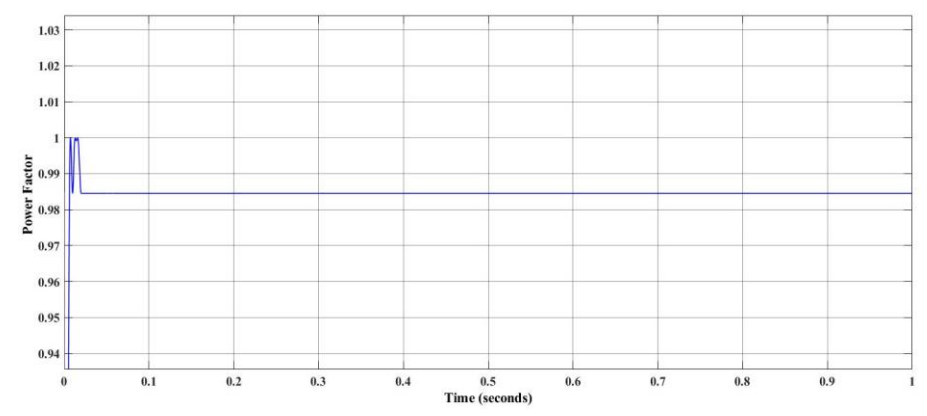


Figure 15: Power factor of the proposed system

Figure 15 shows a power factor of 98.7, indicating exceptionally high efficiency and quantifying the effectiveness of the electrical power. Such a high power factor suggests that the system is well-optimized, reducing the need for additional power factor correction and minimizing energy losses using the proposed converter, which is crucial for operational efficiency and cost-effectiveness. It also implies a minimal phase difference between voltage and current, indicating synchronous peaks typical

2024, 9(4s)

e-ISSN: 2468-4376

https://www.jisem-journal.com/

Research Article

in systems with predominantly resistive loads. Furthermore, harmonic distortion, which might impact the power factor and overall system efficiency, is not considered in the analysis.

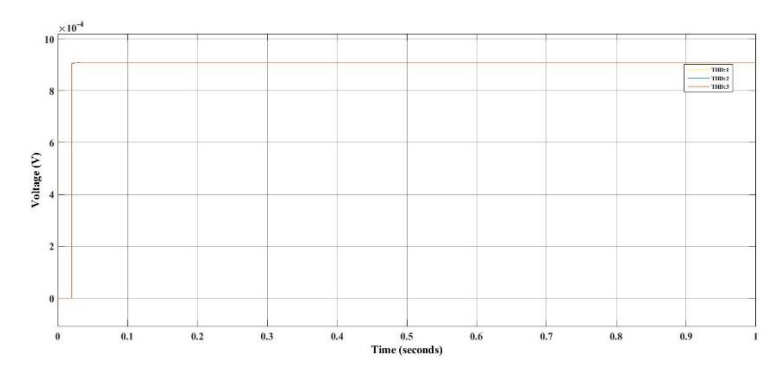


Figure 16: THD waveform based on voltage

The specific voltage value of 0.0009 volts, as shown in Figure 16 is relatively low, which suggests that the harmonic content relative to the fundamental voltage is minimal. The graph likely shows the harmonic voltage components alone, excluding the fundamental frequency's voltage, which would typically be much higher. Consistent low-level harmonics mean that the electrical system maintains high-quality power delivery without significant interference or fluctuations in voltage due to harmonics. Furthermore, the figure isolates harmonic voltage components from the fundamental frequency. However, this separation may miss interactions that impact power quality between harmonics and the fundamental voltage. Periodic increases in harmonic distortion could result from the low harmonic levels suggested, which failed to consider variations over time or under different operating situations. Furthermore, the system may need to incorporate extensive filtering and compensation techniques to achieve and maintain such low harmonic levels, adding to its complexity and expense.

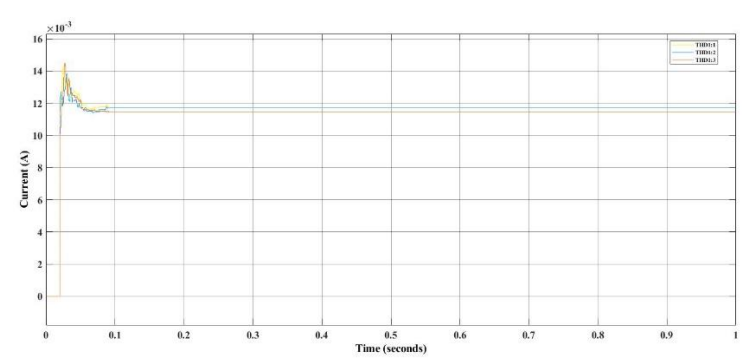


Figure 17: THD waveform based on current

Figure 17, illustrates the magnitude of the harmonic current components about the fundamental current at the stated current value of 0.01157 amperes. Maintaining power quality and equipment dependability depends on the electrical system's capacity to manage and control harmonic currents, which consistent low-level harmonic content implies. Furthermore, the low harmonic current value might be attained in perfect circumstances that might not accurately represent situations where harmonic levels fluctuate.

4.3. Comparative Study

This part compares the performance of the introduced converter with [18], [19], [20] and [21]. Thus, this section provides a comparative analysis of developed high-gain comparable DC-DC CL-based boost topologies after thoroughly investigating the proposed topology. This segment also

2024, 9(4s)

e-ISSN: 2468-4376

https://www.jisem-journal.com/

Research Article

displays that the planned topology is workable. The proposed topology offers many advantages over other topologies published in the most recent and cutting-edge research.

4.3.1. Voltage Gain

The gain in voltage between the suggested model and other models is shown in Figure 18.

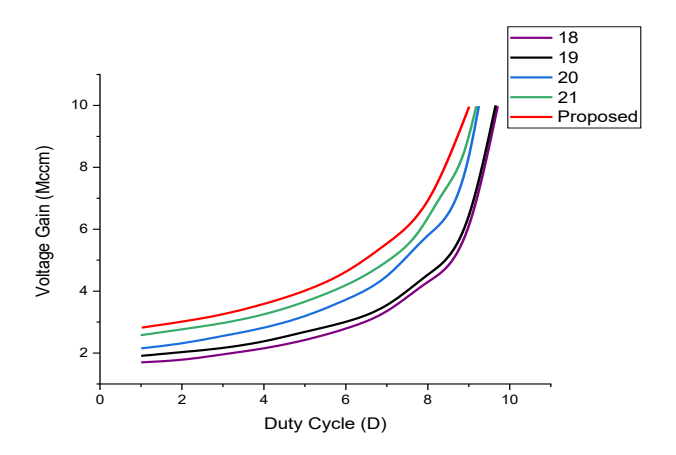


Figure 18: Voltage gain of the proposed model with other models

4.3.2. CCM voltage gain versus duty cycle

When the number of components per CCM voltage gain vs duty cycle is compared, it is vital to notice that the suggested converter has fewer parts than the references and the suggested converter in Figure 19, an inverter without a transformer's front-end boost. The proposed design also incorporates a typical ground relationship between the DC-DC converter's input and output. The recommended structure's continuous input current is another crucial component that qualifies it for use in clean energy presentations. This problem causes leakage inductance in some topologies at the input stage of the structure, where the CL first appears. The leaking inductance will cause the input current to stop flowing.

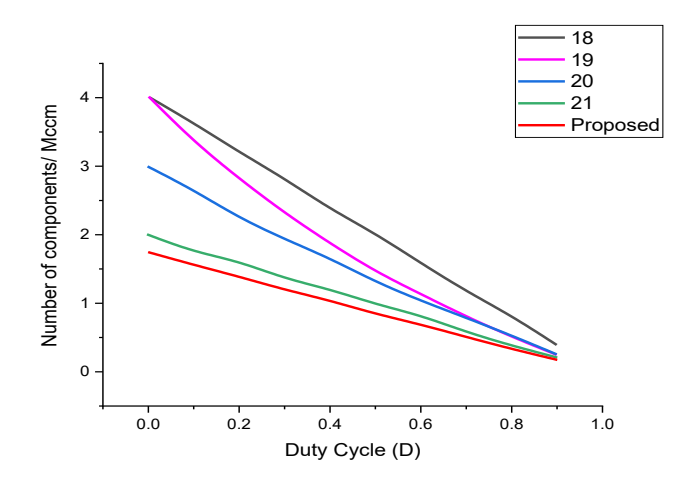


Figure 19: Number of components per CCM voltage gain Vs duty cycle of introduced topology and other topologies

4.3.3. Power switch normalized voltage stress with several structures

According to Figure 20, for any value of D, the primary switching component of the proposed construction is subjected to less normalized voltage stress than the other converters. The

2024, 9(4s) e-ISSN: 2468-4376

https://www.jisem-journal.com/

Research Article

characteristic of the topology is a stable, lowered voltage stress unaffected by D. This has the advantage of allowing the intended topology to use a low RDS (on) resistance and voltage rating MOSFET, which boosts efficiency and lowers costs.

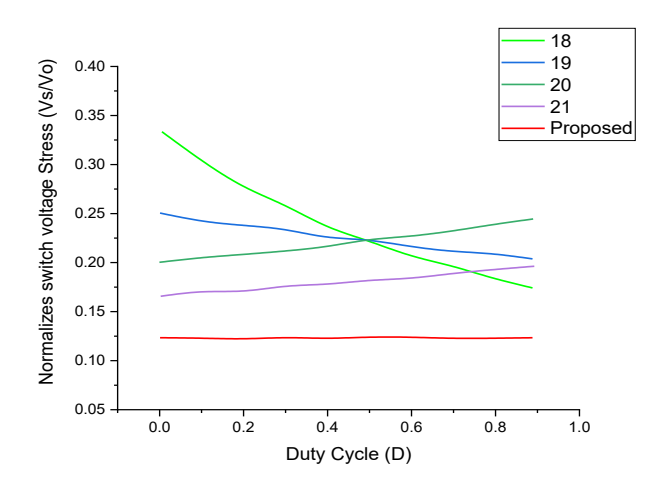


Figure 20: Comparison of Normalized voltage stress with other models

4.3.4. Normalized maximum diode voltage stress:

Figure 21 also displays the normalized maximum diode voltage stress for high step-up converters. Figure 21 demonstrates that the given converter's normalized peak diode voltage stress for all duty cycle values is lesser than that of the additional converters.

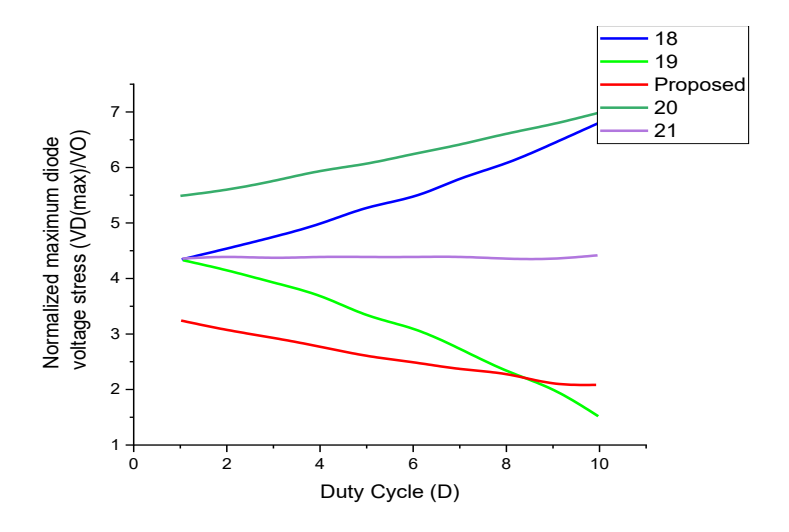


Figure 11: Comparison of normalized maximum diode voltage stress with other models

4.3.5. Theoretical and experimental efficiency:

Figure 22 displays, for various output energy, the efficiency of the new topology as observed empirically and predicted theoretically. The theoretical efficiency curve is produced assuming that the primary power switch and diodes' on-state resistances are 0.01 and 0.04, respectively. According to Figure 24, the most excellent efficiency is 95.9% for 100 W output power and 95.4% for 250 W output power. Due to the impact of core losses, leakage inductance, and additional losses, the observed efficiency is lower than theoretically predicted values.

2024, 9(4s)

e-ISSN: 2468-4376

https://www.jisem-journal.com/

Research Article

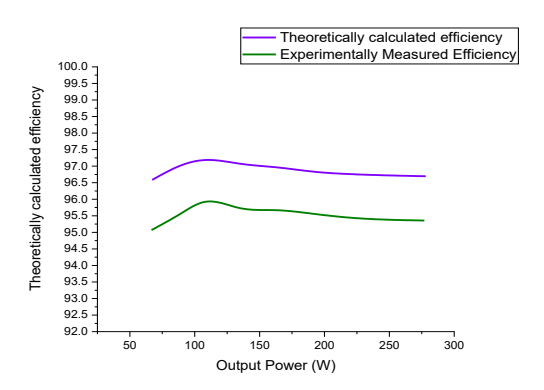


Figure 22: Theoretical and Experimental Efficiency

As a final point, the experimental measurement findings verify the analysis and viability of the topology. The newly developed DC-DC converter is perfect for clean energy tasks, including FCs and PV electrical systems, due to its ultra-high voltage gain, significant effectiveness, repurposed energy, & minimal voltage stress on switching elements.

5. CONCLUSION

In conclusion, the proposed advanced high step-up Zeta converter represents a significant enhancement in DC-DC conversion technology, tailored explicitly for PV applications in grid-connected systems. This converter effectively manages a broad input voltage range by addressing the challenges associated with fluctuating solar energy production, maximizing system efficiency and energy yield. Its near-unity power factor correction ensures optimal power quality. It facilitates seamless grid integration, while its design features, such as ZVS and interleaved operation, minimize voltage spikes, switching noise, and EMI, enhancing system reliability and meeting regulatory standards. Including a PID controller further optimizes voltage output, reduces component stress, and improves overall efficiency. The converter's notable performance metrics are an output voltage of 513V, an output current of 9.15A, power of 4693W, and a power factor of 98.7; THD waveform based on voltage, the current is 0.0009 volts, 0.01157 amperes demonstrate its effectiveness in delivering high-quality power with minimal harmonic distortion. In the future, extensive experimental validation will be conducted to confirm the simulated performance results. This includes building a prototype of the enhanced high step-up Zeta converter and testing it under real-world conditions to assess its efficiency, power quality, and reliability.

REFERENCES

- [1] Yalla, S. P., Subudhi, P. S., & Ramachandaramurthy, V. K. (2022). Topological review of hybrid RES based multi-port converters. *IET Renewable Power Generation*, *16*(6), 1087-1106.
- [2] Abbasi, M., Abbasi, E., & Li, L. (2021). New transformer-less DC-DC converter topologies with reduced voltage stress on capacitors and increased voltage conversion ratio. *IET Power Electronics*, 14(6), 1173-1192.
- [3] Ríos, S. J., Pagano, D. J., & Lucas, K. E. (2021). Bidirectional power sharing for DC microgrid enabled by dual active bridge DC-DC converter. *Energies*, 14(2), 404.
- [4] Xie, H., & Li, R. (2019). A novel switched-capacitor converter with high voltage gain. *IEEE Access*, 7, 107831-107844.
- [5] Kumar, T. P., Mughal, S. N., Deshmukh, R. G., Kumar, S. G., Kumar, Y., & David, D. S. (2022). A highly consistent and proficient class of multiport dc-dc converter based sustainable energy sources. *Materials Today: Proceedings*, *56*, 1758-1768.

2024, 9(4s)

e-ISSN: 2468-4376

https://www.jisem-journal.com/

Research Article

- [6] Abbasi, M., Abbasi, E., Li, L., & Tousi, B. (2021). Design and analysis of a high-gain step-up/down modular DC–DC converter with continuous input current and decreased voltage stress on power switches and switched-capacitors. *Sustainability*, 13(9), 5243.
- [7] Savrun, M. M., & Alihan, A. T. A. Y. (2021). High Voltage Gain Multi-port Bidirectional DC-DC Converter with an Effective Multi-loop Control Strategy for PV/Battery Integrated Systems. *European Mechanical Science*, 5(3), 99-104.
- [8] Li, C., Lu, Z., Zhu, A., Li, C., Luo, H., Li, W., & He, X. (2022). A highly efficient power block with series connection of power SiC MOSFETs-design, characterization and assessment in MV converters. *IET Power Electronics*, 15(7), 605-620.
- [9] Kavipriya, S. (2021). A Novel Bidirectional Soft Switching Dc-Dc Converter. *Turkish Journal of Computer and Mathematics Education (TURCOMAT)*, 12(9), 2824-2827.
- [10] Rahimi, R., Habibi, S., Ferdowsi, M., & Shamsi, P. (2021). An interleaved quadratic high step-up DC-DC converter with coupled inductor. *IEEE Open Journal of Power Electronics*, 2, 647-658.
- [11] Khalili, S., Ahmadi, A. A., Adib, E., & Golsorkhi, M. S. (2023). Single-switch coupled-inductors-based high step-up converter with reduced voltage stress. *IET Power Electronics*.
- [12] Zeng, J., Du, X., & Yang, Z. (2021). A multiport bidirectional DC–DC converter for hybrid renewable energy system integration. *IEEE Transactions on Power Electronics*, 36(11), 12281-12291.
- [13] Xu, X., Bao, G., Ma, M., & Wang, Y. (2021). Multi-Objective Optimization Phase-Shift Control Strategy for Dual-Active-Bridge Isolated Bidirectional DC-DC Converter. *Informacije MIDEM*, *51*(3), 179.
- [14] Salim, K., Asif, M., Ali, F., Armghan, A., Ullah, N., Mohammad, A. S., & Al Ahmadi, A. A. (2022). Low-stress and optimum design of boost converter for renewable energy systems. *Micromachines*, 13(7), 1085.
- [15] Azmoon-Asmarood, S., Maalandish, M., Shoghli, I., Nazemi-Oskuee, S. H. R., & Hosseini, S. H. (2022). A non-isolated high step-up MIMO DC–DC converter for renewable energy applications. *IET Power Electronics*, *15*(10), 953-962.
- [16] Ning, J., Zeng, J., & Du, X. (2019, September). A four-port bidirectional DC-DC converter for renewable energy-battery-DC microgrid system. In *2019 IEEE Energy Conversion Congress and Exposition (ECCE)* (pp. 6722-6727). IEEE.
- [17] Chandran, I. R., & Nallaperumal, C. (2020). A High Voltage Gain Multiport Zeta-Zeta Converter for Renewable Energy Systems. *Informacije MIDEM*, *50*(3), 215-230.
- [18] Khalilzadeh, M., & Abbaszadeh, K. (2015). Non-isolated high step-up DC–DC converter based on coupled inductor with reduced voltage stress. *IET power electronics*, *8*(11), 2184-2194.
- [19] Hu, X., Wang, J., Li, L., & Li, Y. (2017). A three-winding coupled-inductor DC–DC converter topology with high voltage gain and reduced switch stress. *IEEE Transactions on Power Electronics*, 33(2), 1453-1462.
- [20] Nouri, T., Hosseini, S. H., Babaei, E., & Ebrahimi, J. (2015). Interleaved high step-up DC-DC converter based on three-winding high-frequency coupled inductor and voltage multiplier cell. *IET Power Electronics*, 8(2), 175-189.
- [21] Changchien, S. K., Liang, T. J., Chen, J. F., & Yang, L. S. (2009). Novel high step-up DC–DC converter for fuel cell energy conversion system. *IEEE Transactions on Industrial Electronics*, *57*(6), 2007-2017.
- [22] Sutikno, T., Aprilianto, R. A., & Purnama, H. S. (2023). Application of non-isolated bidirectional DC–DC converters for renewable and sustainable energy systems: a review. *Clean Energy*, 7(2), 293-311.
- [23] Sutikno, T., Samosir, A. S., Aprilianto, R. A., Purnama, H. S., Arsadiando, W., & Padmanaban, S. (2023). Advanced DC–DC converter topologies for solar energy harvesting applications: a review. *Clean Energy*, 7(3), 555-570.